REVIEW ARTICLE

MRI OF LYMPHOMAS THROUGH CLINICAL CASES

Obrazowanie chłoniaków metodą rezonansu magnetycznego na podstawie analizy przypadków

Michał Wąsik[1], Kamila Sieradocha[2], Aleksandra Śledziewska[1], Aleksandra Zagajewska[3], Magdalena Cyrkler[1], Dorota Słupik[1], Aleksandra Reda[1], Aleksandra Giba[1], Aleksandra Krygowska[1]

1. *Military Institute of Medicine – National Research Institute, Department of Medical Radiology, Poland*
2. *University Clinical Hospital in Poznań, Poland*
3. *Infant Jesus Clinical Hospital in Warsaw, Poland*

Michał Wąsik – 0009-0007-8163-4265
Kamila Sieradocha – 0009-0006-1952-0139
Aleksandra Śledziewska – 0009-0006-3782-9201
Aleksandra Zagajewska – 0009-0001-8610-0234
Magdalena Cyrkler – 0009-0003-5721-6945
Dorota Słupik – 0009-0006-1818-2684
Aleksandra Reda – 0009-0006-2339-0568
Aleksandra Giba – 0009-0003-2384-1662
Aleksandra Krygowska – 0000-0002-6860-9942

Abstract

Lymphomas are a diverse group of lymphoid neoplasms that can develop in various parts of the body. This paper discusses four clinical cases of patients with lymphomas of the brain, orbit, mesentery and bone, with special emphasis on their morphology on magnetic resonance imaging, emphasizing the importance of this technique in diagnosis and assessment of disease progression. In each case, despite the different histological types, the characteristic imaging features of lymphomas, i.e. signal homogeneity in T1-weighted images, absence of cystic elements, intense contrast enhancement and diffusion restriction, were identified before treatment. Attention is given to the therapeutic implications of early suspicion of lymphoma and the importance of biopsy in confirming the diagnosis. The paper emphasizes that skillful interpretation of MRI images in the context of the overall clinical picture can significantly shorten the diagnostic process and accelerate the implementation of targeted treatment in the affected patients.

Streszczenie

Chłoniaki to zróżnicowana grupa nowotworów limfatycznych, które mogą występować w organizmie w różnych lokalizacjach. W pracy omówiono cztery przypadki kliniczne pacjentów z chłoniakami mózgowia, oczodołu, krezki oraz kości, ze szczególnym uwzględnieniem ich morfologii w obrazowaniu rezonansu magnetycznego, podkreślając znaczenie tej techniki w diagnostyce i ocenie zaawansowania choroby. W każdym przypadku, pomimo różnych typów histologicznych, zidentyfikowano charakterystyczne cechy obrazowe chłoniaków przed rozpoczęciem leczenia, tj. jednorodność sygnału w obrazach T1-zależnych, brak elementów torbielowatych, intensywne wzmocnienie kontrastowe oraz ograniczenie swobodnej dyfuzji wody. Zwrócono uwagę na implikacje terapeutyczne wynikające z wczesnego podejrzenia chłoniaka oraz znaczenie biopsji w ostatecznym potwierdzeniu diagnozy. Praca podkreśla, że umiejętna interpretacja obrazów MRI w kontekście pełnego obrazu klinicznego może znacząco skrócić czas do postawienia diagnozy i przyspieszyć wdrożenie leczenia celowanego u pacjentów z chłoniakami.

Keywords: lymphoma; MRI

Słowa kluczowe: chłoniak; obrazowanie metodą rezonansu magnetycznego

DOI 10.53301/lw/205699

Received: 10.04.2025

Accepted: 29.05.2025

Corresponding author:
Michał Wąsik
Military Institute of Medicine –
National Research Institute, Warsaw
e-mail: michal.michal.w@wp.pl

Introduction

Lymphomas are a heterogeneous group of malignancies arising from lymphocytes, with diverse clinical presentations that can involve any part of the body. They account for approximately 4% of all malignancies diagnosed worldwide [1,2], with this proportion increasing to 15% in the paediatric population [3]. Depending on their site of origin, lymphomas are classified as primary or secondary. Non-invasive imaging techniques, magnetic resonance imaging (MRI) in particular, play a key role in diagnosing and assessing the initial extent of the disease. Knowledge of typical radiological features of lymphomas facilitates timely diagnosis and the initiation of appropriate treatment [3, 4].

Case reports

Case 1

A 39-year-old man presented to the Emergency Department (ED) with a head MRI report indicating an intra-axial mass in the left parietal-occipital region. The imaging had been performed due to headaches and hearing impairment persisting for one month. He also had a history of hypertension, temporarily managed with captopril. A head computed tomography (CT) scan taken on the same day revealed a focal lesion in the left parietal lobe, another in the region of the left lenticular nucleus, as well as soft tissue lesions surrounding the left auditory ossicles and causing their complete destruction.

After excluding the need for urgent neurosurgical intervention, the patient was admitted to the Neurology Clinic for further diagnostic evaluation. Neurological examination found right-sided hemianopia and mild weakness of the right upper limb. The patient received dexamethasone, 20% mannitol, and furosemide, with the head of the bed elevated to 30°.

MRI performed during hospital stay revealed three solid, homogeneous focal lesions in the left cerebral hemisphere, surrounded by Steinhoff grade II vasogenic oedema: two located adjacent to each other at the border of the peripheral parietal and occipital lobes, and one within the deep structures. The lesions showed hypointensity on T1-weighted images relative to white matter, intermediate signal on T2-weighted images, restricted diffusion on diffusion-weighted imaging (DWI) and apparent diffusion coefficient (ADC) maps, intense homogeneous contrast enhancement, and low relative cerebral blood volume (rCBV) on perfusion imaging. Susceptibility-weighted angiography (SWAN) revealed prior punctate microbleeds (Fig. 1).

Multifocal central nervous system (CNS) lymphoma was suspected, and glucocorticoids (GCs) were discontinued. The patient was scheduled for a core needle biopsy (CNB) of the left-sided parietal-occipital tumour; however, the procedure was postponed for 2 weeks due to the 6-day course of steroid therapy. As a result of the treatment used, the patient's condition improved in terms of

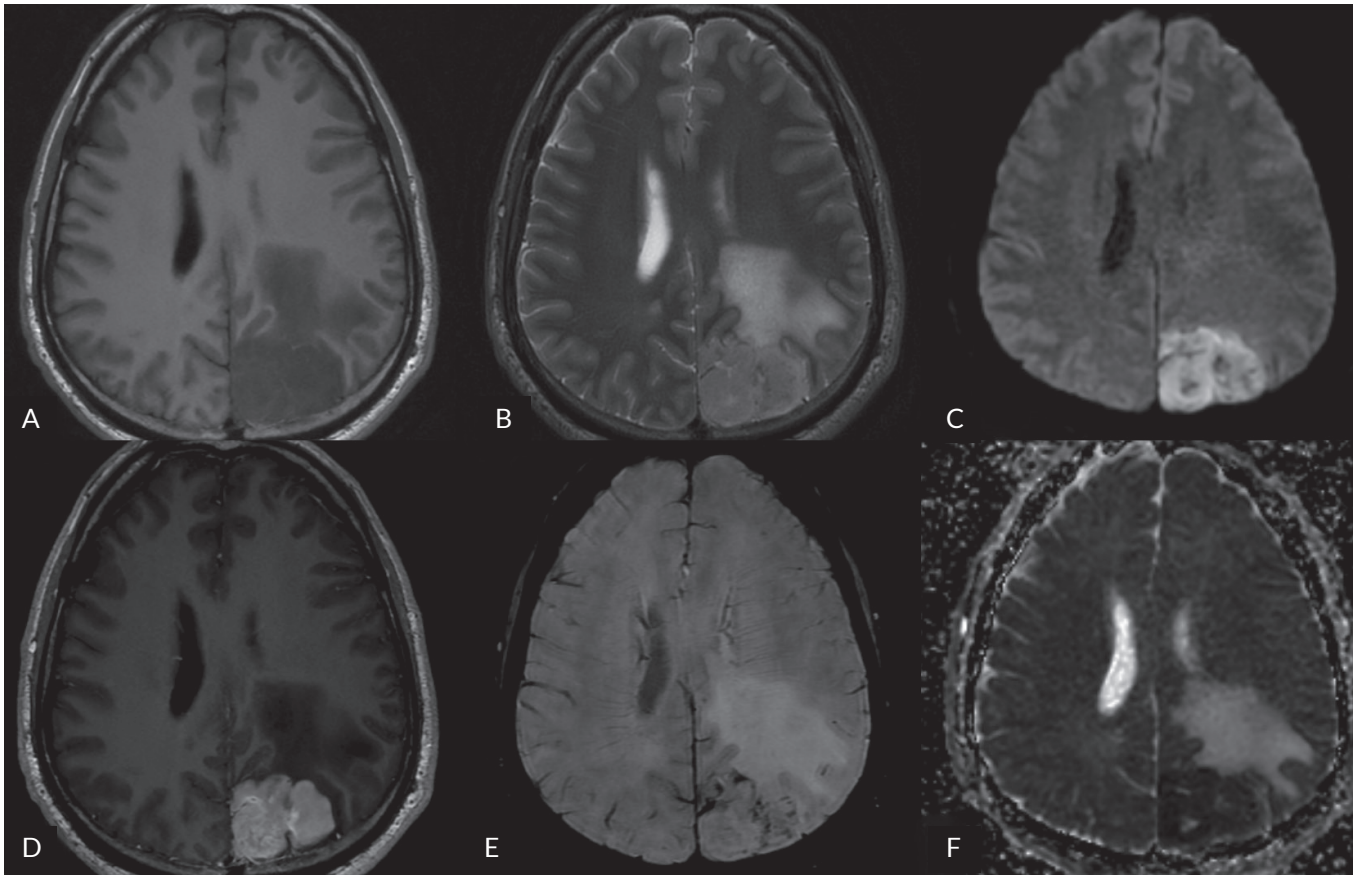

Figure 1. Selected MRI scans of the head, obtained during the patient's initial hospital stay, show two adjacent lymphomas in the left parieto-occipital region. **A.** Pre-contrast T1-weighted image. **B.** T2-weighted image. **C.** DWI image. **D.** Post-contrast T1-weighted image. E. SWAN image. F. ADC map

both subjective and focal symptoms. He was given recommendations and was discharged home in good general condition. Four days later, the patient returned to ED with morning vomiting, worsening headache, and general deterioration. A head CT demonstrated progression in the size of all focal lesions and the surrounding oedema. The patient was admitted to the Department of Neurosurgery, where a repeated head MRI confirmed disease progression (Fig. 2).

CNB was performed earlier than planned, 7 days after the last dose of dexamethasone. Histopathology revealed aggressive infiltration by primary diffuse large B-cell lymphoma of the CNS. The Ki-67 proliferation index exceeded 90%. The patient progressively deteriorated over the following days. He did not survive despite intensified anti-oedema therapy and ventricular drain implantation.

Case 2

A 71-year-old woman presented to the ophthalmology clinic with a sensation of pressure in her left eye socket and drooping of the left upper eyelid. She had a history of hypertension and rheumatoid arthritis (RA), for which she was on regular methotrexate (MTX) therapy. Ophthalmological examination revealed a hard, immobile, bulging mass over the left eyeball, accompanied by ptosis on the same side. Orbital MRI showed a solid, homogeneous, well-defined focal lesion measuring approximately 30 × 35 × 9 mm, located between the levator palpebrae superioris muscle and the left orbital roof. The mass showed marked diffusion restriction and intense contrast enhancement. Its T1-weighted signal intensity was similar to that of the extraocular muscles. There was no invasion of adjacent structures (Fig. 3 and Fig. 4). Based on these findings, orbital lymphoma was suspected. A biopsy of the lesion was performed. Histopathology revealed abundant lymphoid infiltrates, predominantly small B lymphocytes with amorphous nuclei. The Ki-67 proliferative index was 5–10%. These microscopic findings supported the diagnosis of extranodal marginal zone lymphoma (EMZL, mucosa-associated lymphoid tissue, MALT). A suspicion was raised that the lymphoma had developed as a result of the immunosuppressive effects of MTX. The patient was referred to a haematology clinic for further treatment, and showed gradual disease regression on subsequent follow-ups.

Case 3

A 33-year-old man with no significant medical history presented to ED with abdominal pain persisting for one month. Abdominal CT performed a few days earlier at another hospital had shown a small-bowel mesenteric haematoma measuring approximately 5 × 5 × 6 cm. The patient had initially refused hospitalization. Abdomi-

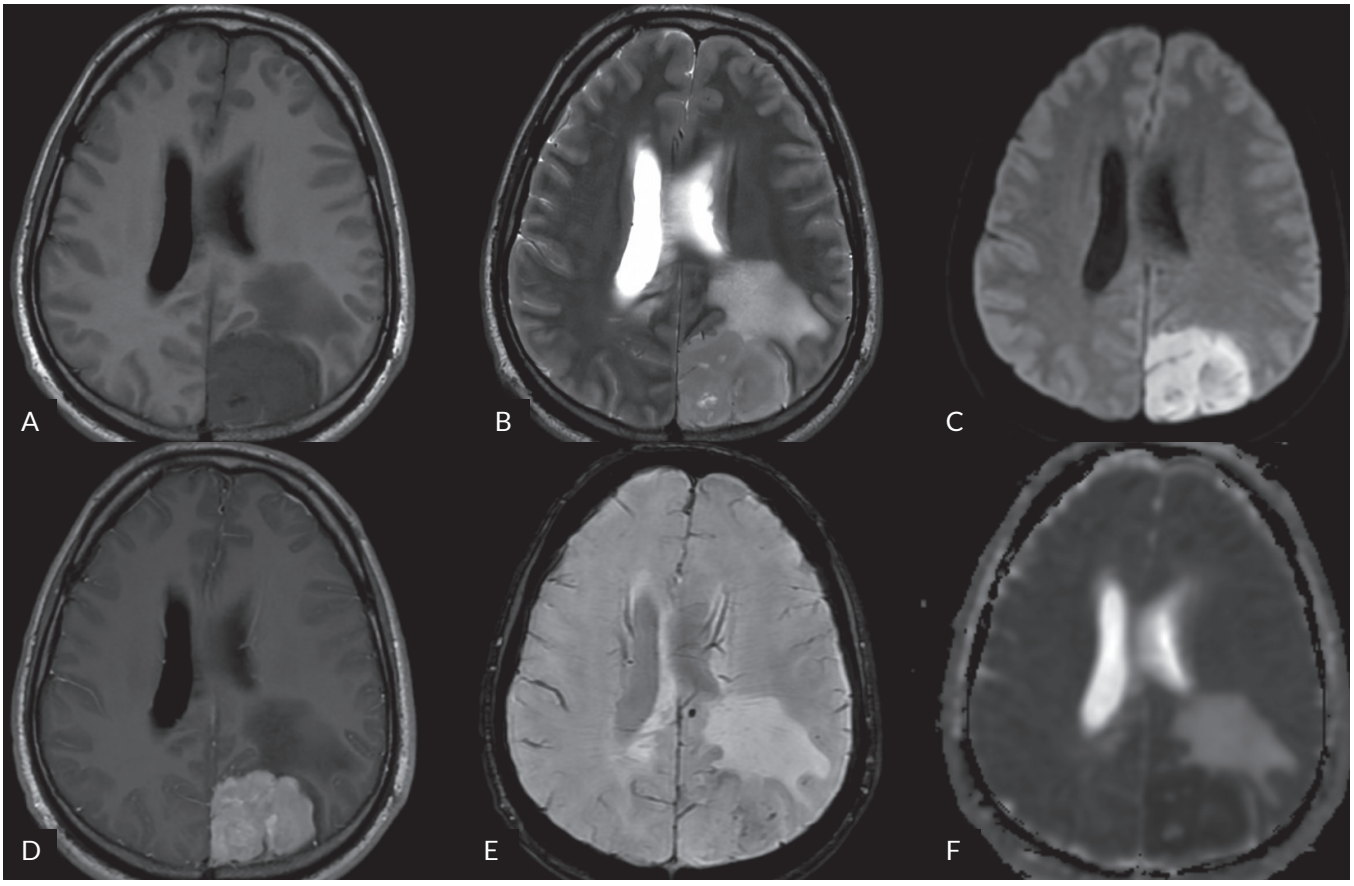

Figure 2. Selected MRI scans of the head, performed during the patient's second admission, show progression in the size of two lymphomas in the left parietal-occipital region, which had already merged into one. Peritumoral oedema is also visible, increased compared to the baseline scan. **A.** Pre-contrast T1-weighted image. **B.** T2-weighted image. **C.** DWI image. **D.** Post-contrast T1-weighted image. **E.** SWAN image. **F.** ADC map

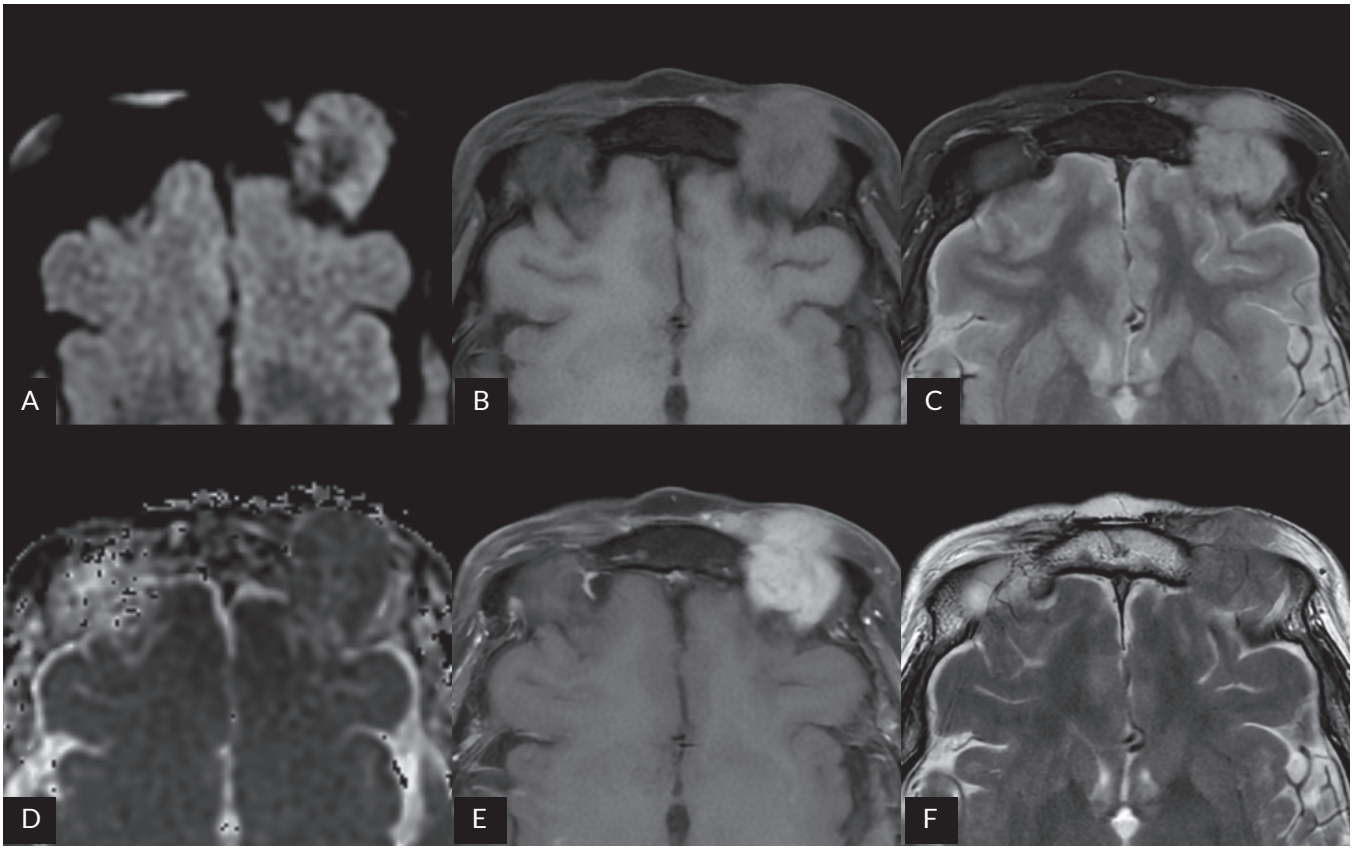

Figure 3. Selected transverse orbital MRI scans demonstrate a lymphoma at the left orbital roof. **A.** DWI image. **B.** Pre-contrast T1-weighted image with fat suppression. **C.** STIR image. **D.** ADC map. **E.** Post-contrast T1-weighted image with fat suppression. F. T2-weighted image

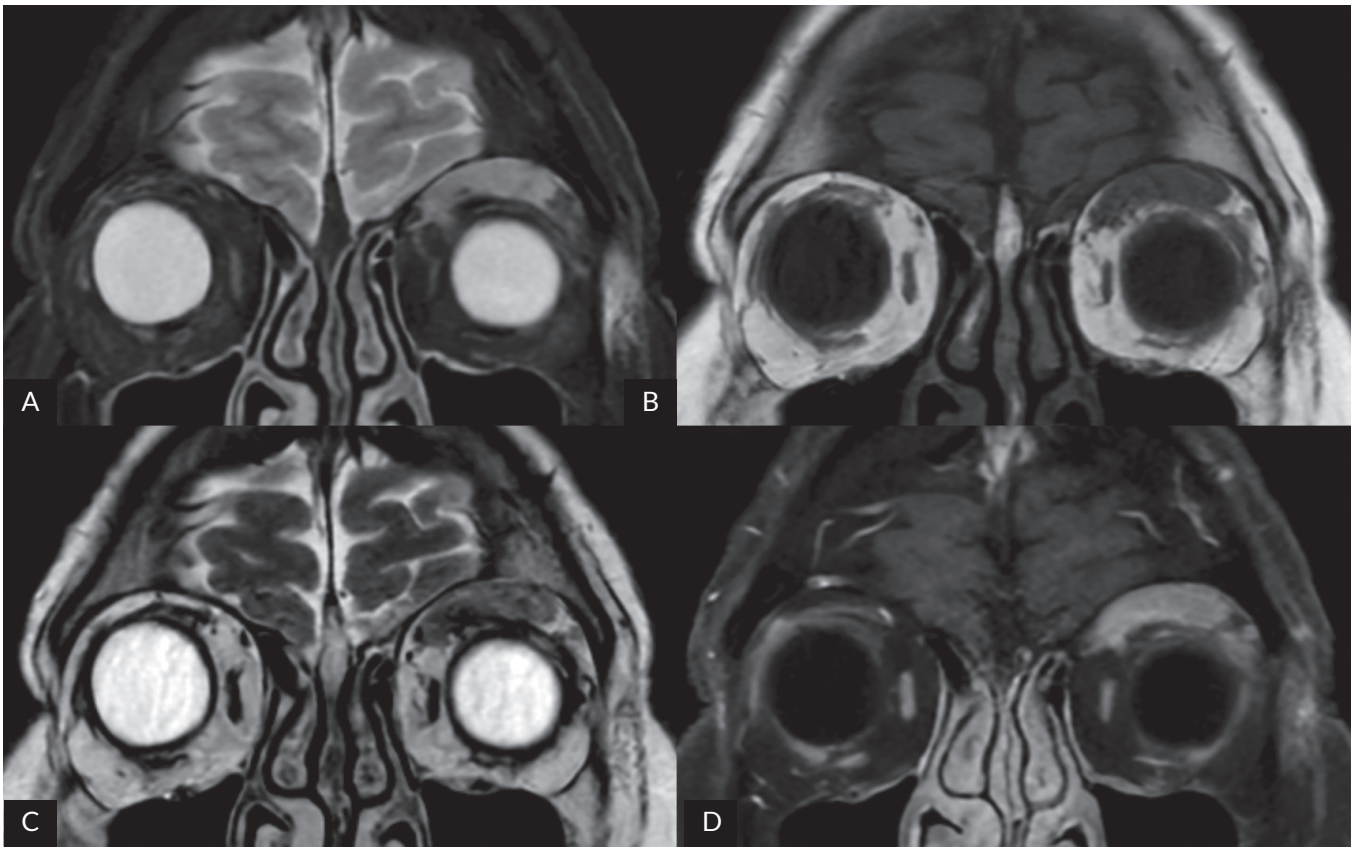

Figure 4. Selected coronal MRI scans of the orbits demonstrate a lymphoma at the roof of the left orbit. **A.** STIR image. **B.** Pre-contrast T1-weighted image without fat suppression. **C.** T2-weighted image. **D.** Post-contrast T1-weighted image with fat suppression

nal US on admission to ED identified a solid intraperitoneal tumour measuring approximately 8 × 10 cm in the left mid-abdomen. The man was admitted to the Department of General and Cancer Surgery for further diagnostic workup and treatment.

Abdominal MRI revealed several solid, relatively homogeneous tumours within the visceral adipose tissue. The largest, measuring approximately 8 × 10 cm, was located in the left small-bowel mesentery. The tumours showed restricted diffusion and marked contrast enhancement, with no cystic components visible (Fig. 5). These findings suggested disseminated lymphoma. Due to increasing pain and clinical manifestations of small-bowel obstruction, laparoscopy with biopsy was performed. Histopathology revealed monomorphic infiltrates of medium-sized lymphoid cells with scant cytoplasm, dispersed nuclear chromatin, several nucleoli, and numerous phagocytic macrophages, giving rise to the characteristic 'starry sky' pattern. The Ki-67 proliferative index was 100%, consistent with Burkitt's lymphoma.

The patient was referred to the Department of Haematology for further treatment. After two cycles of chemotherapy, imaging demonstrated a very good response: the largest lymphoma reduced by more than half, while the remaining lesions regressed completely.

Case 4

A 74-year-old woman presented to the surgical clinic with a slowly enlarging mass in her right axilla. Her sister (at 55 years) and mother (at 77 years) had both been diagnosed with lymphoma in the past. Ultrasound-guided fine-needle aspiration biopsy of the barely palpable right axillary mass was performed. Smears showed multiple small lymphocytes, but no atypical cells. A surgical biopsy of the lymph node group was subsequently performed. Histopathology, along with the overall clinical picture, confirmed the diagnosis of follicular lymphoma with a predominantly diffuse growth pattern (diffuse follicular lymphoma, dFL).

Whole-body positron emission tomography (PET) showed active lymphoproliferative involvement of the right axillary nodes and increased tracer uptake in the medullary cavity of the proximal left femoral shaft. MRI of the left thigh revealed a 15-cm focal lesion, which in some areas occupied the entire width of the femoral medullary cavity. The tumour demonstrated a homogeneous T1-weighted signal (similar to muscle) and an inhomogeneous T2-weighted and short tau inversion recovery (STIR) signal, ranging from intermediate to markedly increased, as well as intense contrast enhancement and restricted diffusion (Fig. 6).

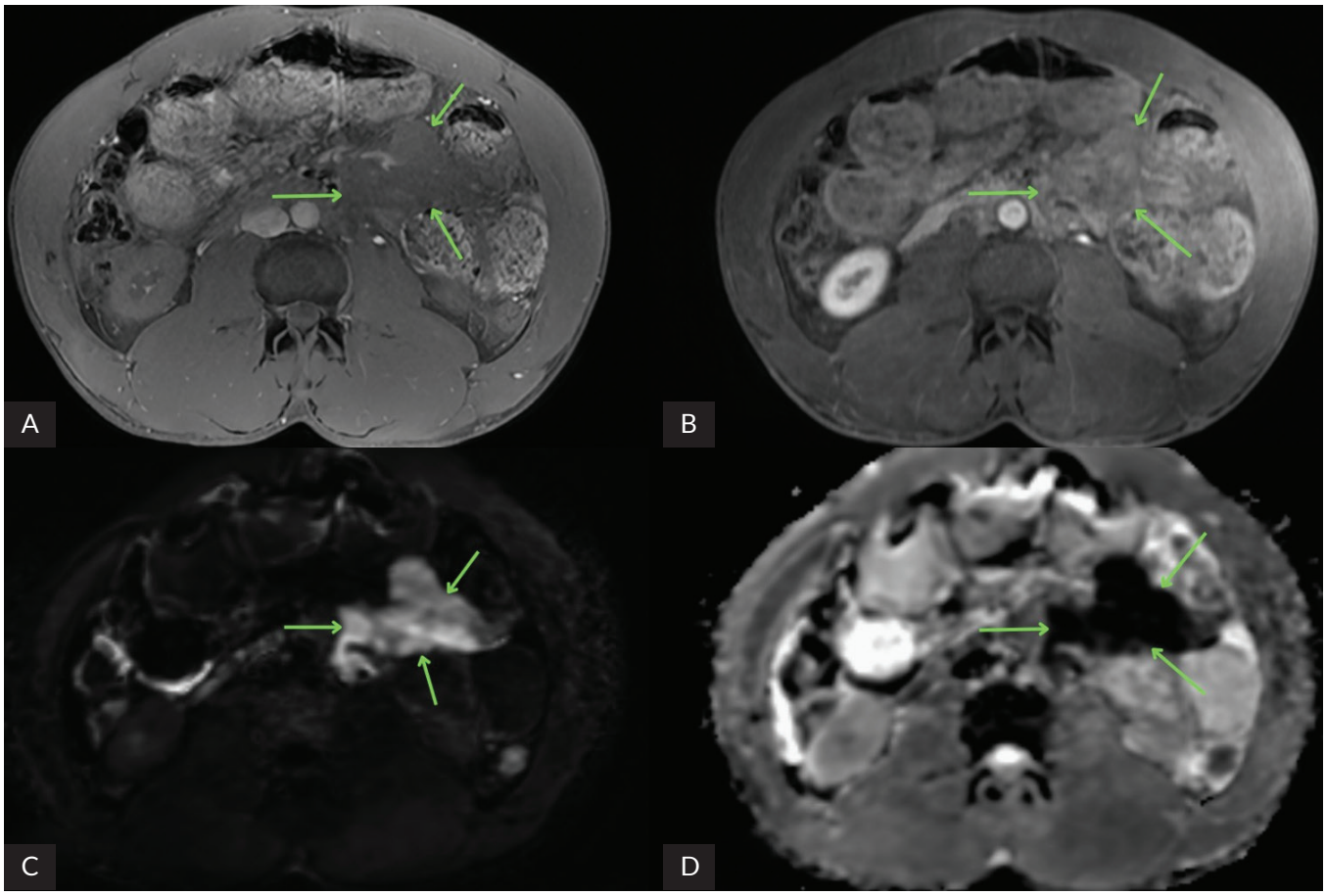

Figure 5. Selected transverse abdominal MRI scans show a lymphoma in the left mesentery of the small intestine (indicated by arrows). **A.** Pre-contrast T1-weighted image with fat suppression; **B.** Post-contrast T1-weighted image with fat suppression; **C.** DWI image; **D.** DC map

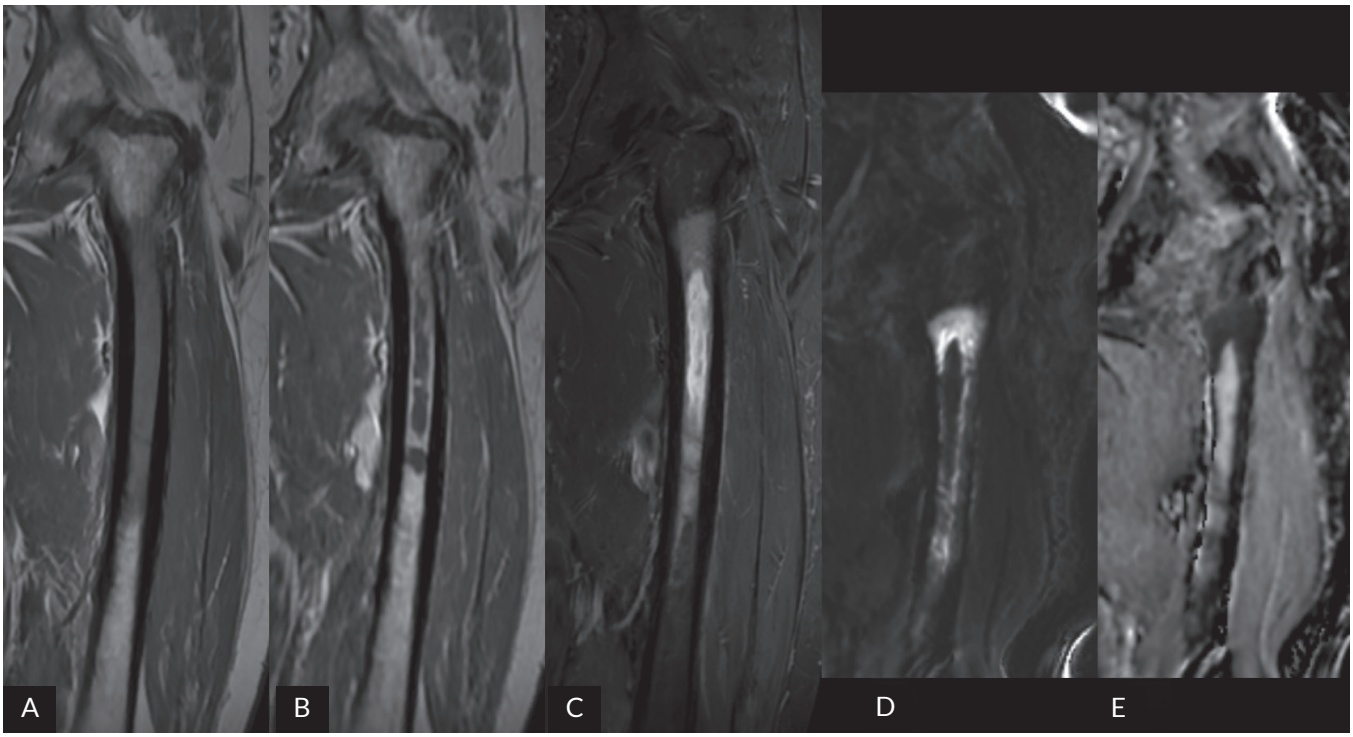

Figure 6. Selected coronal MRI scans of the left thigh show lymphoma involvement of the left femur. **A.** Pre-contrast T1-weighted image. **B.** Post-contrast T1-weighted image. **C.** STIR image. **D.** DWI image. **E.** ADC map

The overall clinical picture suggested a lymphoma involving the proximal left femur. This was confirmed by histopathological evaluation of fluid and curettings from the bone marrow cavity, which revealed cells with an immunophenotype consistent with follicular lymphoma. The patient is currently undergoing chemotherapy.

Discussion

CNS lymphomas are the second most common primary malignant brain tumours after gliomas [5]. Primary diffuse large B-cell lymphoma (DLBCL) is the predominant type, accounting for approximately 85% of cases. On MRI, these tumours typically show no cystic components, appear hypointense relative to surrounding cerebral parenchyma on T2-weighted images, demonstrate restricted diffusion, exhibit intense and relatively homogeneous contrast enhancement, and display low-to-intermediate rCBV values on perfusion imaging [6].

Historically, present or past haemorrhage on SWAN imaging strongly argued against a diagnosis of lymphoma. However, recent reports describe such findings in up to 50% of patients [7, 8].

Preoperative suspicion of lymphoma is crucial for appropriate management. Anti-oedema GC therapy should be withheld until a definitive diagnosis is reached. Immediate biopsy is recommended to promptly initiate chemotherapy rather than to proceed with tumour resection as in other suspected CNS malignancies [6, 7].

Lymphomas account for approximately 55% of all orbital malignancies [9], most commonly arising in the superolateral quadrant [10]. Extranodal marginal zone lymphoma (MALT lymphoma) represents 55–60% of orbital lymphomas [11].

On MRI, they appear as a well-defined, homogeneous, usually lobulated mass surrounding healthy intraorbital structures. They usually do not cause bone destruction. A homogeneous, intermediate T1- and T2-weighted signal is typical, with homogeneous, intense contrast enhancement. Compared to extraocular muscles, lymphomas are iso- or hypointense on T1-weighted images (due to high cell density) and hyperintense on T2-weighted images. High DWI signal and low ADC signal are valuable clues in differentiating lymphomas from inflammatory foci [12].

Burkitt lymphoma is one of the fastest-growing cancers, able to double its cell number within 24–48 hours [13]. In developed countries, its sporadic variant is the most common, accounting for less than 1% of all non-Hodgkin lymphomas in adults. The overall incidence is three cases per million people per year [4]. Patients typically present with massive abdominal masses [15]. Despite their rarity, they cannot be definitively distinguished from other lymphomas using MRI scans alone. These are solid, homogeneous masses, well demarcated from adjacent tissues. They exhibit homogeneous, fairly intense contrast enhancement [16], and restricted diffusion [14, 17].

A thorough evaluation of bone marrow is of paramount importance for staging, as bone marrow involvement (BMI), which is found in 5–15% of patients with Hodgkin's lymphoma (HL) and in 20–40% of patients with non-Hodgkin's lymphoma (NHL), by definition indicates stage

IV disease [1–4]. This fact has both therapeutic and prognostic implications [5, 6].

Lymphoma infiltrates the bone marrow, forming channels in the cancellous bone and penetrating between fibrous areas. MRI is the most sensitive tool for detecting these tumours. DWI images allow for assessing bone marrow infiltration at an earlier stage than other sequences. All MRI sequences show abnormal bone marrow signal. T1-weighted images typically exhibit uniformly low signal intensity, isointense relative to muscle. Greater signal variability is seen on STIR images, which demonstrate areas of high, intermediate, or low intensity [18]. Other notable MRI features suggestive of bone lymphoma include concomitant involvement of surrounding soft tissues with minimal destruction of the cortical bone, marked oedema, absence of necrosis or bleeding, and intense enhancement following intravenous contrast [19].

Normal, hypercellular lymphatic organs (e.g., spleen, lymph nodes, and tonsils) physiologically demonstrate increased DWI signal and decreased ADC signal compared to adjacent tissues [20, 21] (Fig. 7). Therefore, simply identifying an area or structure meeting these two criteria does not always constitute a basis for suspecting lymphoma. A thorough knowledge of anatomy and histology is crucial in this case to avoid misinterpretation of a normal image as a pathological one and, consequently,

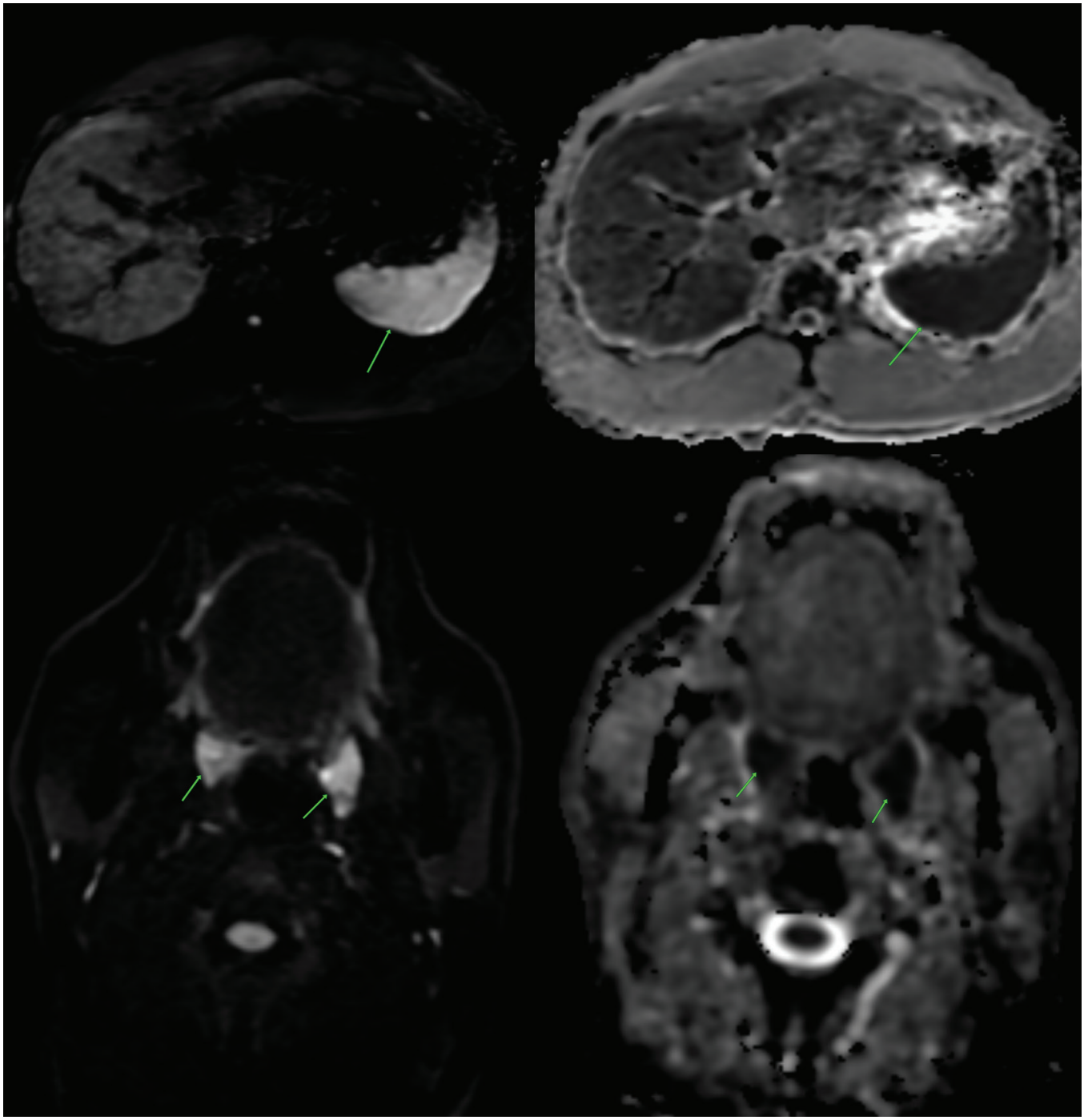

Figure 7. Images show physiological homogeneous diffusion restriction on DWI images and ADC map in normal spleen (marked with arrows at the top) and palatine tonsils (marked with arrows at the bottom)

exposing patients to unnecessary further diagnostic workup and anxiety.

Conclusions

Despite their diverse clinical presentation, lymphomas, regardless of their location, share several common MRI features, such as homogeneous T1-weighted signal, the absence of a fluid component within the tumour, limited diffusion, and intense, homogeneous contrast enhancement. However, it is important to remember that none of these features, or even their coexistence, is pathognomonic for lymphoma. Correct MRI interpretation and correlation with the clinical presentation can shorten the diagnostic path for patients with lymphoma and allow for earlier initiation of targeted therapy.

References

1. Huang J, Pang WS, Lok V, et al.; NCD Global Health Research Group, Association of Pacific Rim Universities (APRU). Incidence, mortality, risk factors, and trends for Hodgkin lymphoma: a global data analysis. J Hematol Oncol, 2022; 15: 57. doi: 10.1186/s13045-022-01281-9
2. Thandra KC, Barsouk A, Saginala K, et al. Epidemiology of Non-Hodgkin's lymphoma. Med Sci (Basel), 2021; 9: 5. doi: 10.3390/medsci9010005
3. Toma P, Granata C, Rossi A, Garaventa A. Multimodality imaging of Hodgkin disease and non-Hodgkin lymphomas in children. Radiographics, 2007; 27: 1335–1354. doi: 10.1148/rg.275065157
4. Frampas E. Lymphomas: Basic points that radiologists should know. Diagn Interv Imaging, 2013; 94: 131–144. doi: 10.1016/j.diii.2012.11.006
5. Miller KD, Ostrom QT, Kruchko C, et al. Brain and other central nervous system tumor statistics, 2021. CA Cancer J Clin, 2021; 71: 381–406. doi: 10.3322/caac.21693
6. Pons-Escoda A, Naval-Baudin P, Velasco R, et al. Imaging of lymphomas involving the CNS: an update-review of the full spectrum of disease with an emphasis on the World Health Organization Classifications of CNS tumors 2021 and hematolymphoid tumors 2022. AJNR Am J Neuroradiol, 2023; 44: 358–366. doi: 10.3174/ajnr.A7795
7. Velasco R, Mercadal S, Vidal N, et al.; GELTAMO and GENOSEN group. Diagnostic delay and outcome in immunocompetent patients with primary central nervous system lymphoma in Spain: a multicentric study. J Neurooncol, 2020; 148: 545–554. doi: 10.1007/s11060-020-03547-z
8. Sakata A, Okada T, Yamamoto A, et al. Primary central nervous system lymphoma: is absence of intratumoral hemorrhage a characteristic finding on MRI? Radiol Oncol, 2015; 49: 128–134. doi: 10.1515/raon-2015-0007
9. Margo CE, Mulla ZD. Malignant tumors of the orbit. Analysis of the Florida Cancer Registry. Ophthalmology, 1998; 105: 185–190. doi: 10.1016/s0161-6420(98)92107-8
10. Priego G, Majos C, Climent F, Muntane A. Orbital lymphoma: imaging features and differential diagnosis. Insights Imaging, 2012; 3: 337–344. doi: 10.1007/s13244-012-0156-1
11. Richards H, Ramsden C, Naidoo R, et al. Ocular adnexal lymphomas: a review. Expert Rev Ophthalmol, 2017; 12: 133–148. doi: 10.1080/17469899.2017.1280394
12. Vogele D, Sollmann N, Beck A, et al. Orbital tumors-clinical, radiologic and histopathologic correlation. Diagnostics (Basel), 2022; 12: 2376. doi: 10.3390/diagnostics12102376
13. Schmitz R, Ceribelli M, Pittaluga S, et al. Oncogenic mechanisms in Burkitt lymphoma. Cold Spring Harb Perspect Med, 2014; 4: a014282. doi: 10.1101/cshperspect.a014282
14. Kalisz K, Alessandrino F, Beck R, et al. An update on Burkitt lymphoma: a review of pathogenesis and multimodality imaging assessment of disease presentation, treatment response, and recurrence. Insights Imaging, 2019; 10: 56. doi: 10.1186/s13244-019-0733-7
15. Siddiqui SH, Thakral B, Aakash F, et al. From the archives of MD Anderson Cancer Center: Sporadic Burkitt lymphoma with a complex karyotype and SOX11 expression. Ann Diagn Pathol, 2023; 66: 152182. doi: 10.1016/j.anndiagpath.2023.152182
16. Karaosmanoglu AD, Uysal A, Onur MR, et al. Primary lymphomas of the intraabdominal solid organs and the gastrointestinal tract: spectrum of imaging findings with histopathological confirmation. Abdom Radiol (NY), 2019; 44: 2988–3005. doi: 10.1007/s00261-019-02100-5
17. Derinkuyu BE, Boyuna a Ö, Öztunalı Ç, et al. Imaging features of Burkitt lymphoma in pediatric patients. Diagn Interv Radiol, 2016; 22: 95–100. doi: 10.5152/dir.2015.15211
18. Murphey MD, Kransdorf MJ. Primary musculoskeletal lymphoma. Radiol Clin North Am, 2016; 54: 785–795. doi: 10.1016/j.rcl.2016.03.008
19. Steffner RJ, Jang ES, Danford NC. Lymphoma of bone. JBJS Rev, 2018; 6: e1. doi: 10.2106/JBJS.RVW.17.00006
20. Khoo MM, Tyler PA, Saifuddin A, Padhani AR. Diffusion-weighted imaging (DWI) in musculoskeletal MRI: a critical review. Skeletal Radiol, 2011; 40: 665–681. doi: 10.1007/s00256-011-1106-6
21. Donners R, Yiin RSZ, Koh DM, et al. Whole-body diffusion-weighted MRI in lymphoma-comparison of global apparent diffusion coefficient histogram parameters for differentiation of diseased nodes of lymphoma patients from normal lymph nodes of healthy individuals. Quant Imaging Med Surg, 2021; 11: 3549–3561. doi: 10.21037/qims-21-50